

Transition Processes in Mach 6.8 Boundary Layers at Varying Temperature Conditions Investigated by Spatial Direct Numerical Simulation

A. Fezer, M. Kloker

Universität Stuttgart, Institut für Aerodynamik und Gasdynamik (IAG)
Pfaffenwaldring 21, D-70550 Stuttgart, Germany

Summary

Spatial direct numerical simulations (DNS) are carried out to investigate laminar-turbulent transition scenarios under varying temperature conditions of the oncoming flow, distinguishing wind-tunnel and flight conditions. First, Linear Stability Theory is used for both cases to get an overview of the primary stability behaviour of the flat-plate boundary layer where different disturbance modes have to be regarded. Simulations have been performed for fundamental and oblique breakdown in both cases. The investigation of the streamwise amplitude development in connection with the corresponding wall-normal disturbance profiles gives information about which types of modes interact to eventually trigger laminar-turbulent breakdown. The results allow estimations of the probability of the different transition scenarios in practice.

Introduction

Laminar-turbulent transition is of great importance for high-speed aerospace vehicles, because heat flux and shear stresses change significantly during the transition process, leading to strong thermal stresses at turbulence. The knowledge of transition in compressible boundary layers is, compared to the incompressible case, rather incomplete due to the great difficulties in achieving valuable experimental results. Except for some investigations using Linear Stability Theory (LST), almost all results were achieved for "cold" flow, i.e. at flow conditions of wind-tunnel experiments. As Stetson [7] stated after a 10-year experimental research program to investigate the stability of a Mach 6.8 cone boundary layer, results obtained in these experiments are not directly reliable to flight conditions because of the different stability properties of the flows. Therefore direct numerical simulations are a valuable tool to explore transition processes at flight conditions. As a first, important work in this direction, Eglior [3] and Bestek & Eglior [2] investigated at IAG the temperature effects in Mach 4.8 boundary layers. One main conclusion was that the "hot" flow is not necessarily more stable (as widely assumed for simplification) if a realistic wall-cooling by radiation is taken into account. Moreover, the (weakly) nonlinear mechanisms setting the stage for the transition downstream can be different.

The simulations presented here aim at investigating the spatial instability and the laminar-turbulent transition of Mach 6.8 boundary-layer flows along a flat plate. They can be understood as numerical simulations of "controlled" transition experiments. Temporally periodic 2-d and 3-d disturbances with fixed frequency and amplitude are induced, and the reaction of the boundary layer, i.e. the spatial development of the disturbance waves,

is simulated by numerical solution of the complete, three-dimensional, unsteady, compressible Navier-Stokes equations.

Numerical method

The flow is considered in a rectangular integration domain (Fig. 1) on the flat plate, not containing any shock wave induced by the leading edge. In a disturbance strip at the wall artificial 2-d and 3-d disturbances are excited by blowing and suction. At the end of the integration domain a buffer domain is appended ($x_3 \leq x \leq x_N$), in which all disturbances of the flow are smoothly damped to zero in order to avoid spurious reflections from the outflow boundary.

The equation of continuity, the Navier-Stokes equations and the energy equation are used in conservative form for the variables ρ , ρu , ρv , ρw and ρe , solved in a disturbance formulation [3]. Lengths are non-dimensionalized with respect to a reference length L . Reference values for velocities, temperature, viscosity, conductivity and density are their freestream values (indicated by subscript ∞). The pressure is normalized with $\rho_\infty^* u_\infty^{*2}$ and the internal energy with u_∞^{*2} , where the superscript * denotes the dimensional quantities. With these definitions, the global and local Reynolds numbers are

$$Re = \frac{u_\infty^* L \rho_\infty^*}{\mu_\infty^*} = 10^5, \quad Re_x = \frac{u_\infty^* x^* \rho_\infty^*}{\mu_\infty^*} = x \cdot Re = Re_x^2. \quad (1)$$

The fluid is considered as nonreacting, perfect gas, for which the thermodynamic equation of state is valid. The modelling of the thermodynamic properties of air is implemented for *colorimetrically perfect gas* as well as for *thermally perfect gas* [1, 2, 3].

In streamwise direction the spatial discretization is performed by 4th-order accurate compact finite differences with high modal resolution, which are used in a splitted form. The advantages of split-type compact schemes are discussed in detail by Kloker [5]. Central (viscous terms) and alternating upwind/downwind (convective terms) standard differences [3, 4, 8] are used in normal direction. In spanwise direction the flow is assumed to be periodic, so it is suitable to use a Fourier spectral approach

$$f(x, y, z, t) = \sum_{k=-K}^K F_k(x, y, t) e^{ik\beta z} \quad (2)$$

with the basic spanwise wavenumber β . The time integration is performed by a 4-step Runge-Kutta scheme of 4th-order accuracy. A description of the numerical method in more detail is given in [3, 2].

Linear stability analysis of the Ma=6.8 flat-plate boundary layer

First, an overview over the stability behaviour of the $Ma = 6.8$ flat-plate boundary layer shall be worked out with the aid of LST. With this method amplification rates for small disturbances within the relevant frequency parameter range are determined, distinguishing between cold and hot conditions. Following Mack [6] we define wind-tunnel conditions by the following: The stagnation temperature is held constant at $T_0 = 311$ K until, with increasing Mach number, the freestream temperature T_∞ drops below 50 K. For higher

mach numbers, including 6.8, T_∞ is held constant at 50 K and T_0 increases. For flight conditions we choose $T_\infty = 220$ K, which corresponds to the atmosphere temperature at an altitude of about 25 km. At cold conditions we assume an adiabatic wall (thus $T_w = 480$ K), and at hot conditions a realistic, cooled wall with $T_w = 975$ K due to the high adiabatic wall temperatures (> 1900 K).

Figs. 2 and 3 show curves of neutral stability as a function of the local Reynolds number R_z and the frequency parameter $F = \omega/Re = 2\pi f^* L / (\%_\infty Re)$. Within the area enclosed by the curves small perturbations are amplified, outside they are damped. In the wind-tunnel case (Fig. 2) 2-d waves are amplified as 1st and 2nd mode (Tollmien-Schlichting and acoustic mode respectively), but the instability regions of the modes are melted to one coherent region. 3-d waves are not amplified as 1st mode only, analogous to hot conditions. In the latter case 2-d waves are not amplified as 1st mode anymore and the instability region extends to higher dimensionless frequencies. The amplification region of 3-d modes is shifted to higher Reynolds numbers, but the critical Reynolds number (the location where amplification occurs first) nearly keeps constant.

The shown stability diagrams do not contain information about the magnitude of the amplification. Therefore the amplification rates for 6 selected disturbance waves are shown in Fig. 4. For 2-d waves it is obvious that the maximum amplification is relatively large and occurs at relatively high frequency parameters. In these cases, however, growth holds only in small downstream intervals, so the integral amplification is low. Since compressible flat-plate boundary layers are inviscidly unstable, i.e. unstable for $R_z \rightarrow \infty$, waves at special (low) frequencies can theoretically have infinite integral amplification rates, in spite of small local rates. For direct numerical simulations a compromise between these two extremes seems to be appropriate. So the dimensionless disturbance frequency for 2-d waves was set to $F = 10 \cdot 10^{-5}$. As can be suspected by comparison of corresponding cases at cold and hot flow (Fig. 4), atmosphere conditions in connection with wall cooling lead to a destabilization of the 2-d 2nd mode (maximum as well as integral), whereas 3-d modes may be stabilized. So it can be expected that 2-d modes will be involved in the transition process at flight conditions.

Results of direct numerical simulations

Exploiting the results of the previous section, parameters have been chosen to simulate fundamental and oblique breakdown at wind-tunnel and atmosphere conditions. These are given in Tab. 1. As for the wall boundary conditions, a radiation-adiabatic wall-temperature boundary condition for the total flow has also been implemented (see [2, 3]); that, however, is not used here to keep correspondence to the LST calculations.

The disturbance strip is in all cases situated roughly at the begin of the linearly unstable region. The following discussion is based on a temporal Fourier decomposition of the unsteady simulation results over the last calculated time period. We use the notation (h, k) for the resulting Fourier modes, describing a wave with frequency $h \cdot f_0$ and wavenumber $k \cdot \beta$. In the fundamental cases the modes (1,0) (2-d, primary wave) and (1,±1) (3-d symmetric part wave, in the following referred to as (1,1)) are disturbed with the same frequency. In the simulations of oblique breakdown only (1,1) is excited.

Fig. 6 shows the downstream development of the maximum amplitudes (over y) of $(\rho u)'$, considering the most relevant modes for the simulation of fundamental resonance at wind

Tab. 1: Simulation parameters

Simulation	\mathcal{F}_{WT}	\mathcal{F}_{AT}	\mathcal{O}_{WT}	\mathcal{O}_{AT}
T_∞ [K]	50	220	50	220
T_w [K]	484	975	484	975
	adiabatic	cooled	adiabatic	cooled
$F_{(1,0)} \cdot 10^5$	10.0	10.0	—	—
$F_{(1,1)} \cdot 10^5$	10.0	10.0	5.0	2.0
β	11.0	11.0	9.75	4.33
Θ		$\approx 45^\circ$		$\approx 60^\circ$
L [mm]	51.5	17.5	51.5	17.5

tunnel conditions (case \mathcal{F}_{WT}). Only a very weak resonant (1,1)-growth, relevant at a 2-d threshold amplitude of almost 30% at $x \approx 15.6$, can be observed, and no initiation of transition is expected. In the corresponding simulation at atmosphere conditions (case \mathcal{F}_{AT}) comparable maximum 2-d amplitudes occur; the induced resonant growth (starting at $x \approx 23.8$) however is significantly stronger, so that the fundamental 3-d wave amplitude reaches about 18%. Simultaneously, a considerable damping of the 2-d mode (1,0) takes place, probably caused by a stabilization effect of the strong mean flow distortion (0,0) up to 17%. This seems to be a *self-induced suppression* or *delay* of the transition process, in accordance with the general observation in experiments and simulations that the way to full breakdown in hypersonic boundary layers appears to be the longer the higher the Mach number is. Although the disturbance modes keep a high amplitude level (over 10%), the final breakdown stage is slow. This is verified by looking at characteristic flow structures. A suitable quantity for visualization is the vorticity ω . Fig. 12 shows contour lines of the instantaneous z -component of the vorticity $\omega_z = \frac{\partial u}{\partial y} - \frac{\partial v}{\partial x}$ in the plane $z = \lambda/2$ in case \mathcal{F}_{AT} . This representation makes it possible to locate high-shear layers which play a dominant role in the transition process. The region shown extends to approximately four wave lengths. Developed high-shear layers are visible which periodically travel downstream. They remind of the structures connected with the forming of A-vortices in incompressible flow just prior to full breakdown. However, the present structures "ride" downstream, but there is no rapid decay that typically exists in incompressible transitional boundary layers starting from the tip of a Λ -vortex.

Nevertheless, it is rather unexpected that, in spite of such high amplitudes of the 2-d disturbance, virtually no resonance appears in the wind-tunnel case. A check of the phase speeds of the disturbance waves (not shown here) reveals no synchronisation which is necessary for the resonance mechanism. To further examine this phenomena we look at the amplitude distributions in wall-normal direction at approximately the x -position where the (1,0)-threshold amplitude is reached ($R_z = 1250$ for wind-tunnel and $R_z = 1450$ for atmosphere conditions). The results from LST (in this terminology called eigenfunctions) are shown in Fig. 5. Although the theory is not valid in the nonlinear regime, it is instructive to recall the different kind the modes look like. As mentioned before, the instability regions of 2-d 1st and 2nd mode merge in the wind-tunnel case, so the eigenfunction constitutes a synthesis of both modes (WT, $\Theta = 0^\circ$). However, the dominating part is of 2nd mode, visible from the strong near-wall maximum, which is intensified in streamwise direction. The 3-d wave, on the other hand, is a pure 1st mode (WT, $\Theta \approx 45^\circ$). At hot

conditions we have a pure 2^{nd} mode 2-d wave (AT, $\Theta = 0^\circ$) and a mixed-mode 3-d wave (AT, $\Theta \approx 45^\circ$).

We now examine the amplitude distributions of mode (1,1) from the numerical simulations (Fig. 8 and 9). In both cases the amplitude distribution at the first plotted x -position looks much like the one from LST. In the wind-tunnel case there is a second maximum far from the wall which does not fit to the LST profile. This is due to a further mode (to make things worse) stimulated by the disturbance strip, a so-called *multiple viscous mode*, which is strongly damped and disappears soon. Further downstream the shape of the distribution stays the same; the wave remains 1^{st} mode. At hot conditions we find a different behaviour. When the 2-d wave reaches its amplitude maximum, the 1^{st} -mode part of the profile disappears and the mode (1,1) looks much like a pure 2^{nd} mode, caused by the resonant interaction with the (1,0) acoustic mode. Hence it is clear that both primary and secondary wave have to be of nearly the same mode type to yield resonance. The question remains whether both modes must have (at least partly) the same identity before the position where the threshold amplitude is reached, or under which circumstances the secondary wave can mutate to the other mode identity.

While in the fundamental case transition is initiated by resonant interaction of a primary 2-d 2^{nd} mode disturbance with a secondary 3-d disturbance, it is caused in the oblique breakdown by nonlinear processes of 3-d 1^{st} mode disturbances alone. This kind of transition was first discovered and investigated by Thumm [8] at IAG. In the simulations presented here the (1,1)-mode has been disturbed at frequencies and spanwise wave lengths for which LST-predicted amplification is strongest (see Tab. 1). In the cold case this disturbance is amplified only in a finite area at comparatively high rates according to LST, whereas in the hot case we have a wide range of instability with nearly constant, but low amplification rates (see Figs 2-4); the Re_x -regions of the simulations have been chosen correspondingly. The maximum amplitudes resulting from the simulations are plotted in Fig. 10 (wind-tunnel cond., case O_{WT}) and Fig. 11 (atmosphere cond., case O_{AT}). During oblique breakdown only modes (h, k) with even sum $h+k$ are nonlinearly generated as well as $(0,0)$. In both cases the directly nonlinearly generated mode $(0,2)$ increases strongly and generates, together with the initial disturbance $(1,1)$, the modes $(1,3)$ and $(1,5)$. The plots show that the oblique-type breakdown is a robust mechanism at wind-tunnel as well as at flight conditions. This is due to the fact that neither a phase speed synchronisation process nor a threshold amplitude are required. The (1,1)-growth according to the LST results, stronger in the wind-tunnel case, and amplitude saturation starts early. In the hot case, the growth is slower as expected. As can be seen from the ω_z vorticity iso-contours of case O_{AT} (Fig 13), the structure deformation in the oblique-type breakdown is much faster (relative to the primary wavelength) and of another type than in the fundamental mechanism.

Conclusions

Linear-Stability-Theory results show a destabilization of the high-frequency acoustic 2-d 2^{nd} mode disturbances at flight conditions if realistic wall cooling is considered. In the simulations of fundamental breakdown for wind-tunnel and atmosphere conditions, comparable disturbances lead to significant fundamental resonance only at atmosphere conditions. As the reason for the resonance deficiency at wind-tunnel conditions the different mode identity of the primary (2^{nd} mode) and secondary (1^{st} mode) disturbance wave has

been found. At hot conditions a self-induced stabilization occurred at a certain disturbance level, caused by a strong mean-flow distortion, which may delay or even suppress the transition process. Oblique-type transition proves to be a robust mechanism, even at high temperatures, where 3-d modes are, according to linear theory, less amplified. The financial support of the Deutsche Forschungsgemeinschaft (DFG) within Sonderforschungsbereich 259, Project C4, is gratefully acknowledged.

References

- [1] J.D. Anderson. *Hypersonic and high temperature gas dynamics*. McGraw-Hill Book Company, 1989.
- [2] H. Bestek and W. Eißler. DNS of Transition in Mach 4.8 Boundary Layers at Flight Conditions. In G. Betgeles W. Rodi, editor, *Engineering Turbulence Modelling and Experiments 3*. Elsevier Science B.V., 1996.
- [3] W. Eißler. *Numerische Untersuchungen zum laminar-turbulenten Strömungsumschlag in Überschallgrenzschichten*. Dissertation, Universität Stuttgart, Stuttgart, Germany, 1995.
- [4] D. Gortlieb and E. Turkel. Dissipative two-four methods for time-dependent problems. *Math. Comp.*, 30:703-723, 1976.
- [5] M. Kloker. A Robust High-Resolution Split-Type Compact FD-Scheme for Spatial Direct Numerical Simulation of Boundary-Layer Transition. In *Applied Scientific Research 59 (4)*, pages 355-377. Kluwer Acad. Publishers, NL, 1998.
- [6] L.M. Mack. Boundary-layer linear stability theory. In R. Michel, editor, *Special Course on Stability and Transition of Laminar Flow*. AGARD-Report-709, pages 3.1-3.81, 1984.
- [7] K.F. Stetson. Hypersonic transition testing in wind tunnels. In M.Y. Hussaini and R.G. Voigt, editors, *Instability and Transition*, volume 1, pages 91-100. Springer-Verlag, New York, 1990.
- [8] A. Thumm. *Numerische Untersuchungen zum laminar-turbulenten Strömungsumschlag in transsonischen Grenzschichtströmungen*. Dissertation, Universität Stuttgart, Stuttgart, Germany, 1991.

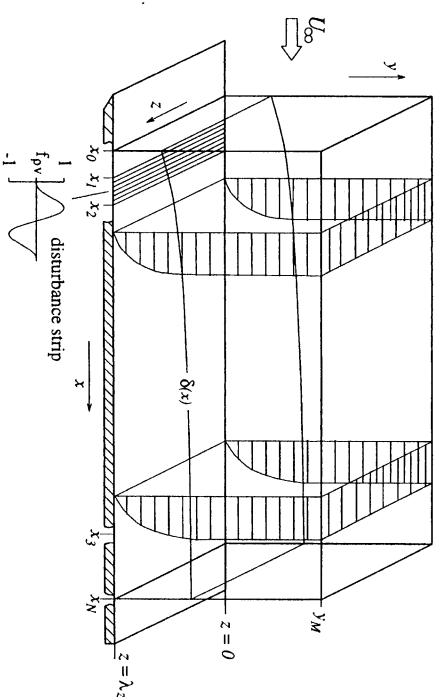


Fig. 1: Integration domain

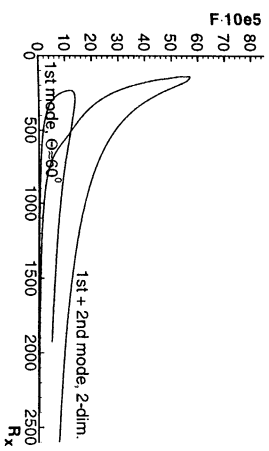


Fig. 2: Neutral stability curves; wind-tunnel conditions, adiabatic wall ($T_w = 480$ K).

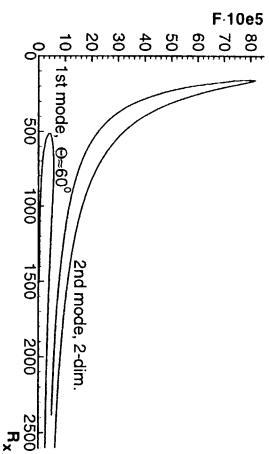


Fig. 3: Neutral stability curves; atmosphere conditions, cooled wall ($T_w = 975$ K).

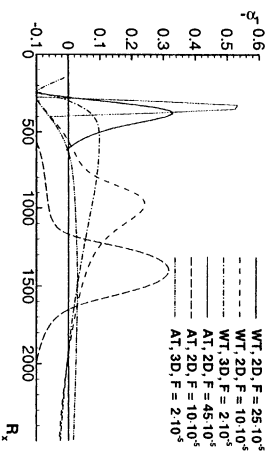


Fig. 4: Amplification rates for selected cases at wind-tunnel (WT) and atmosphere (AT) conditions; 3-d waves with $\Phi \approx 60^\circ$.

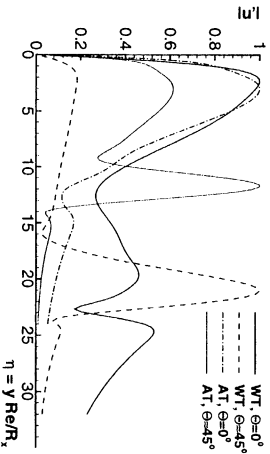


Fig. 5: Normalized eigenfunctions of disturbances at $F = 10 \cdot 10^{-5}$; $Re_x = 1250$ (WT) or $Re_x = 1450$ (AT).

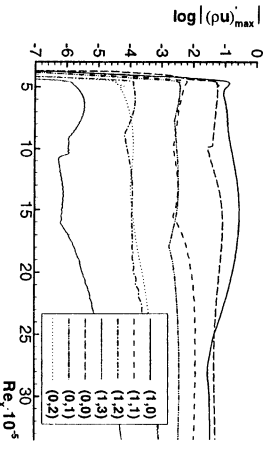


Fig. 6: Downstream development of the $|(\rho u)_{h,k}|$ disturbance amplitudes; wind-tunnel conditions, fundamental-type disturbance combination (case \mathcal{F}_{WT}).

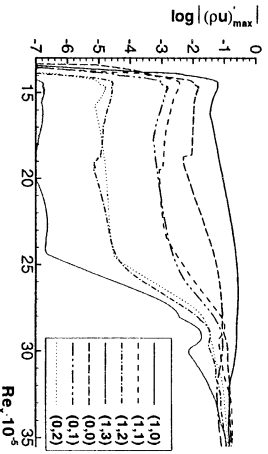


Fig. 7: Downstream development of the $|(\rho u)_{h,k}|$ disturbance amplitudes; atmosphere conditions, fundamental-type disturbance combination (case \mathcal{F}_{AT}).

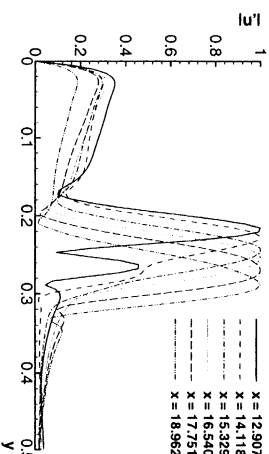


Fig. 8: Normalized amplitude distributions of $u_{(1,1)}$ at various x -positions; wind-tunnel conditions, fundamental-type disturbance combination (case \mathcal{F}_{WT}).

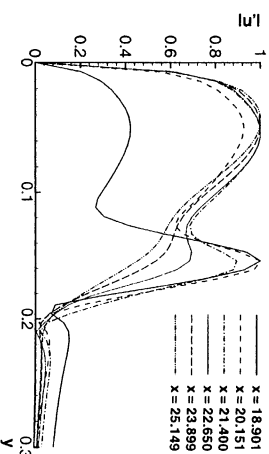


Fig. 9: Normalized amplitude distributions of $u_{(1,1)}$ at various x -positions; atmosphere conditions, fundamental-type disturbance combination (case \mathcal{F}_{AT}).

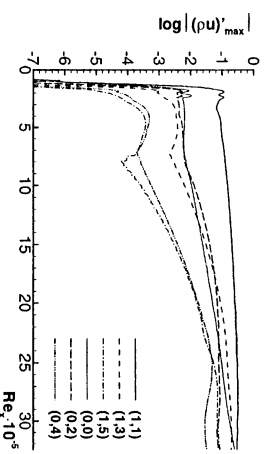


Fig. 10: Downstream development of the $|(\rho u)_{h,k}|$ disturbance amplitudes; wind-tunnel conditions, oblique-type disturbance combination (case \mathcal{O}_{WT}).

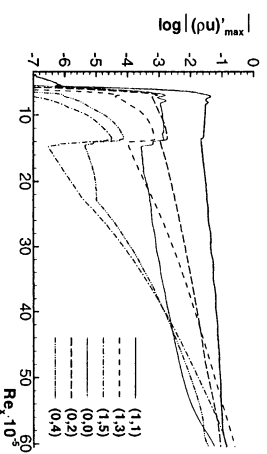


Fig. 11: Downstream development of the $|(\rho u)_{h,k}|$ disturbance amplitudes; atmosphere conditions, oblique-type disturbance combination (case \mathcal{O}_{AT}).

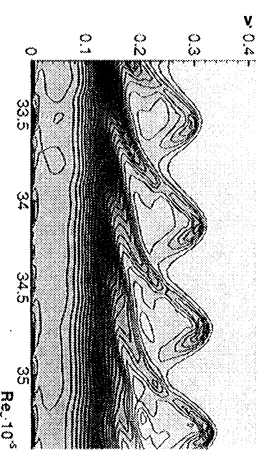


Fig. 12: Iso-contours of the instantaneous vorticity ω_z ; atmosphere conditions, fundamental-type disturbance combination (case \mathcal{F}_{AT}).

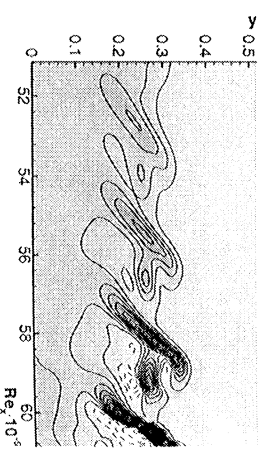


Fig. 13: Iso-contours of the instantaneous vorticity ω_z ; atmosphere conditions, oblique-type disturbance combination (case \mathcal{O}_{AT}).